Physica 147A (1987) 387–406
North-Holland, Amsterdam

LIGHT SCATTERING FROM THE LIQUID–VAPOR INTERFACE

Eric MAZUR and Doo Soo CHUNG
Department of Physics and Division of Applied Sciences, Harvard University, Cambridge, MA 02138, USA

This paper presents light scattering spectra from the liquid–vapor interfaces of water and ethanol. Both quasi-elastic (Rayleigh) scattering and inelastic (Brillouin) scattering from fluctuations at the interface are observed. The spectra were obtained using a novel Fourier transform heterodyne technique that allows one to resolve the full Rayleigh–Brillouin triplet. Capillary waves travelling in opposite directions can therefore be separated, making the present technique suitable for studying nonequilibrium effects in interfaces.

1. Introduction

The macroscopic behavior of an interface between bulk phases has been studied extensively both experimentally and theoretically for a considerable time[1–4]). Most of the work treats the interface away from the critical point as a discontinuous step-like transition between two bulk phases. More recently, however, several theoretical papers have appeared that analyze the hydrodynamic behavior of an interface by including some surface structure[5–7]). For example, Bedeaux and Oppenheim[6]) derived a phenomenological correction to the dispersion relation for surface waves on a fluid. They also predicted a broadening of the Rayleigh peak due to a new purely damped nonpropagating surface mode.

At the same time, there has been growing interest in the behavior of fluids in nonequilibrium states[8,9]). Linear-response theory[10]), fluctuation theory[11]), and kinetic theory[12]) have been applied to the description of uniform fluids out of equilibrium. A predicted asymmetry in the heights of the two Brillouin peaks of light scattered from a fluid subject to a small temperature gradient was experimentally verified[13,14]). The asymmetry is a result of broken time-reversal symmetry. An analogous asymmetry in the intensities of the Brillouin peaks has been derived recently for a planar liquid surface in the presence of a small temperature gradient[15,16]). Light scattering from bulk nonequilibrium liquids presents considerable experimental difficulty, since the nonequilibrium state

0378-4371/87/$03.50

generally results in a nonuniformity in index of refraction. This problem does not occur in light scattering from a liquid–vapor interface.

To observe the low-frequency spectra of fluctuations on liquid–vapor interfaces a high spectral resolution is required. By detecting the beating signal between the scattered laser light and a "local oscillator" field derived from the same laser, resolving powers of 10^{14} have been obtained. This light-beating technique[17]) has been used from the early days of the laser to study light scattering from thermally excited fluctuations (capillary waves) on liquid surfaces[18,19]). The dispersion of capillary waves was measured to determine surface tension and shear viscosity[20]). These techniques were later applied to study the behavior of the liquid–vapor interface near the critical point[21–23]). Light-beating spectroscopy has also been used to study quasi-elastic Rayleigh scattering from bulk liquids[24,25]).

In this paper we present recent measurements of the spectrum of light scattered by a liquid–vapor interface. The following section briefly reviews the relevant theory of hydrodynamic surface modes that contribute to the scattering of incident laser light. Section 3 discusses a novel approach to light-beating spectroscopy involving a direct fast Fourier transform of the detector signal (Fourier transform heterodyne spectroscopy), which is more convenient than the conventional techniques using a spectrum analyzer or autocorrelator. When the local oscillator is frequency-shifted, the full Rayleigh–Brillouin triplet can be resolved, with a directional separation of the Brillouin doublet. Sections 4 and 5 discuss the experiment, and in section 6 we present the first results of a preliminary analysis of some of our data. In the final section we summarize the experimental results and present an outline of the experimental work in progress.

2. Spectrum of hydrodynamic interfacial modes

The description of light scattering from bulk fluids is generally well understood. Many articles and books on this subject have appeared[26]), and most aspects have been experimentally verified. In general, for a given optical geometry, the spectrum of light scattered from a fluid consists of three Lorentzian lines: a central, unshifted Rayleigh peak, and two symmetrically shifted side peaks (Brillouin peaks). The former is due to nonpropagating entropy fluctuations, the latter to propagating density fluctuations. The theoretical analysis of light scattering from an interface[6,27]) is more complicated than that from a bulk phase, mainly due to the lower symmetry of the system. A second complication arises from the description of the interface itself. Most analyses consider a step-like transition between the two phases. It

is well known, however, that the actual interface is diffuse, with a thickness on the order of a nanometer (away from the critical region). Several recent papers deal with this specific problem by separating the system into two bulk phases, liquid and vapor, and an "interface", i.e. an inhomogeneous layer of a certain thickness that separates the two phases. Even though the detailed results of the analyses depend on the model used for the interface, the basic features may be obtained from the linearized hydrodynamic equations and a proper set of boundary conditions. In what follows we present a brief discussion of the features that are relevant for this paper.

Consider a light wave of frequency ω and wavevector $\boldsymbol{k}_0$ incident on the interface between two phases, as in fig. 1. For a perfectly flat boundary between two phases with different indices of refraction, the light beam will be specularly reflected and refracted according to Snell's law. Fluctuations in the interface, however, also cause both elastic and inelastic scattering. Let us write the total entropy, S_T, of a one-component liquid–vapor system as

$$S_T = \int_{V^v} S^v \, d\boldsymbol{r} + \int_{V^i} S^i \, d\boldsymbol{r} + \int_{V^\ell} S^\ell \, d\boldsymbol{r} , \tag{2.1}$$

with S the entropy density, and V the volume; the superscripts v, ℓ and i denote vapor, liquid, and interface, respectively. In this form there are contributions to the total entropy fluctuations, δS_T from fluctuations δS^v, δS^i, and δS^ℓ, and from fluctuations in the position of the interface around its equilibrium position, which enter expression (2.1) through the boundaries of

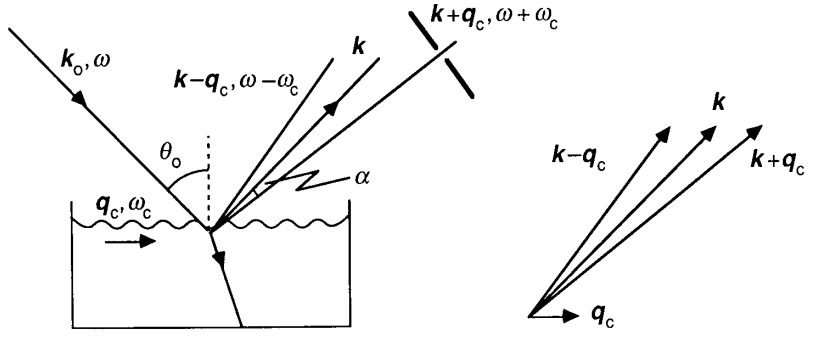

Fig. 1. Optical geometry for measuring spectra from liquid–vapor interfaces. An incident light wave with wavevector $\boldsymbol{k}_0$ and frequency ω strikes the surface under an incidence angle θ_0, and scatters from a capillary wave with wavevector $\boldsymbol{q}_c$ and frequency ω_c. The scattering angle α of the inelastically scattered light determines $\boldsymbol{q}_c$ by the phase-matching condition. Behind the pinhole the spectrum consists of a central Rayleigh peak at ω, and for the capillary wave shown, a single Brillouin peak at $\omega + \omega_c$.

the volume integrations. Position fluctuations are characteristic for a system with an interface, and include surface waves such as capillary and gravity waves. Both the position fluctuations, as well as the entropy fluctuations produce propagating and nonpropagating modes that in turn cause inelastic and quasi-elastic scattering. Because the thickness of the interface is much smaller than the wavelength of the light, position fluctuations dominate in the scattering of the light from an interface.

Quasi-elastic scattering. Just as in the bulk, nonpropagating, purely damped modes cause Rayleigh scattering in all directions. The scattered light is broadened by the damping of the fluctuations. So far, nonpropagating surface modes have been studied only theoretically. According to ref. 6 a dispersion relation for these modes is

$$\omega_R = i\beta^2[(\eta^v\rho^v)^{-1/2} + (\eta^\ell\rho^\ell)^{-1/2}]^2 , \tag{2.2}$$

where ω_R is the frequency mode, β a coefficient of sliding friction between the two phases, η the shear viscosity and ρ the density. Note that the wavevector does not enter this expression. The broadening of the Rayleigh scattering is determined by β and the product of viscosity and density for each of the phases. One therefore expects large differences between liquid–liquid and liquid–vapor interfaces.

Inelastic scattering. The propagating surface modes correspond to gravity waves for long wavelength and capillary waves for small wavelength. The dispersion relation for these waves, which can be obtained from classical hydrodynamic theory[2,3], is

$$\omega_c = [gq + \sigma q^3/\rho^\ell]^{1/2} + 2iq^2\eta^\ell/\rho^\ell , \tag{2.3}$$

with g the acceleration due to gravity, σ the surface tension, and q the wavevector of the surface wave. First order corrections to this relation were obtained by considering interfacial structure[6]).

In this work we are mainly dealing with the short wavelength capillary waves. For a capillary wave with wavevector $\boldsymbol{q}_c$ and frequency ω_c, as in fig. 1, inelastic light scattering will occur in two directions. The scattering angle α is determined by energy and momentum conservation, $\boldsymbol{k}' = \boldsymbol{k} \pm \boldsymbol{q}_c$ and $\omega' = \omega \pm \omega_c$, with $\boldsymbol{k}'$ and ω' the wavevector and frequency of the scattered light. For the situation illustrated in fig. 1, with capillary waves propagating in one direction only, the spectrum at an angle α below the specular reflection will

consist of a single Brillouin peak at $\omega + \omega_c$. In equilibrium, however, there are an equal number of capillary waves propagating in opposite directions, so that the spectrum in any given direction will show two symmetric Brillouin peaks around a central unshifted Rayleigh peak.

Recently, the spectral density of capillary waves in nonequilibrium was obtained from standard linearized hydrodynamics, by introducing random fluctuations of the stress tensor[15,16]). It was shown that if there is a small temperature gradient along a liquid–vapor interface, the Brillouin spectrum becomes asymmetric. This occurs since there are no longer equal number of capillary waves travelling in opposite directions. By separating the two Brillouin peaks in the spectrum of light scattered from a nonequilibrium liquid–vapor interface one could therefore study the nonequilibrium dynamics of a liquid without the difficulties encountered in bulk liquids[13,14]).

3. Optical correlations and hydrodynamic fluctuations

In this section we shall describe the relationship between the detected signal and the hydrodynamic fluctuations and briefly discuss the Fourier transform heterodyne technique. Let the light field be described by $E(t)$. The quantity detected in an experiment is the intensity

$$I(t) = \frac{c\varepsilon_0}{2} E^*(t)E(t) , \tag{3.1}$$

with c the speed of light and ε_0 the dielectric constant. The time dependence of the intensity is averaged over the detector response time τ_d. The detector signal $j_d(t)$ is therfore proportional to the short-time average of the intensity $I(t)$,

$$j_d(t) \propto \frac{1}{2\tau_d} \int_{-\tau_d}^{\tau_d} E^*(t + t')E(t + t') \, dt' . \tag{3.2}$$

Since τ_d is typically on the order of 1 ns, the signal is averaged over the rapid oscillations of the light wave. The techniques to determine the spectrum of the incident light fall in two categories: predetection and postdetection filtering[28]). In the first case one first spectrally filters the incident light, and then measures the spectral intensity. Examples are spectrometers and interferometers, which have a spectral resolution up to 1 MHz. The measured optical power spectrum is related to the first-order or field correlation function

$$G^{(1)}(\tau) = \lim_{T\to\infty} \frac{1}{2T} \int_{-T}^{T} E^*(t)E(t+\tau)\,\mathrm{d}t = \langle E^*(t)E(t+\tau)\rangle\,, \tag{3.3}$$

which in turn is related to the correlation function of the hydrodynamic fluctuations.

In postdetection filtering, such as heterodyne spectroscopy, the total intensity is first detected and the detector signal $j_d(t)$ is later filtered and processed. The spectral range has an upper limit of about 1 GHz, corresponding to the instrumental time resolution. In this type of detection one measures the second-order or intensity correlation function

$$G^{(2)}(\tau) = \langle E^*(t)E(t)E^*(t+\tau)E(t+\tau)\rangle = \frac{4}{c^2\varepsilon_0^2}\langle I(t)I(t+\tau)\rangle\,. \tag{3.4}$$

Let us now consider more explicitly the case of an incident light field of the form

$$E_L(t) = \varepsilon_L\, \mathrm{e}^{-\mathrm{i}\omega_L t + \mathrm{i}\psi(t)}\,, \tag{3.5}$$

with ε_L the amplitude and ω_L the frequency of the light and $\psi(t)$ a slowly varying random function representing the fluctuating phase of the light. The scattered light can be written in the form

$$E_S(t) = f(t)E_L(t)\,, \tag{3.6}$$

where the complex quantity $f(t)$ is a stochastic quantity representing the hydrodynamic fluctuations in the scattering medium. The phase fluctuations limit the spectral resolution of conventional predetection filtering techniques, because the fluctuations contribute to the field correlation function according to

$$G^{(1)}(\tau) = \langle E_S^*(t)E_S(t+\tau)\rangle \sim \langle \mathrm{e}^{-\mathrm{i}[\psi(t)-\psi(t+\tau)]}\rangle\langle f^*(t)f(t+\tau)\rangle\,. \tag{3.7}$$

The spectrum of the scattered light, which is the Fourier transform of $G^{(1)}(\tau)$, is therefore in part determined by the phase fluctuations in the incident field. This is equivalent to saying that whenever the spectral width of the incident field is larger than the width associated with the scattering process, the field correlation function of the scattered light and hence the optical spectrum is dominated by the fluctuations in $\psi(t)$. As can easily be verified from eq. (3.4), however, the phase fluctuations cancel in the *intensity* correlation function if the different components of the macroscopic electric field are coherent. The

spectral resolution of detection techniques involving intensity correlations are therefore not limited by the spectral width of the incident light, but by the spatial coherence of the incident laser light.

In the present detection scheme, the detector is illuminated simultaneously by the scattered light, E_S, and by a local oscillator signal, coherent with the incident laser field and frequency-shifted by an amount ω_{AO},

$$E_{LO}(t) = \varepsilon_{LO}\, e^{-i(\omega_L + \omega_{AO})t + i\psi(t)} . \tag{3.8}$$

The instantaneous intensity at the detector is then

$$I(t) = \frac{c\varepsilon_0}{2} |E_S(t) + E_{LO}(t)|^2 . \tag{3.9}$$

In a stationary case, if $|E_{LO}(t)|^2 \gg |E_S(t)|^2$, neglecting the time independent terms[17]),

$$G^{(2)}(\tau) = \langle E_{LO}(t) E^*_{LO}(t+\tau) E^*_S(t) E_S(t+\tau) \rangle + \text{c.c} . \tag{3.10}$$

Substituting the expressions for the fields, one obtains

$$G^{(2)}(\tau) = \frac{1}{c\varepsilon_0} I_{LO} \langle f^*(t) f(t+\tau) \rangle\, e^{-i\omega_{AO}\tau} + \text{c.c.} , \tag{3.11}$$

with I_{LO} the average intensity of the local oscillator. The quantity of interest is the power spectrum of the stochastic hydrodynamic fluctuations

$$S_f(\omega) = \int_{-\infty}^{\infty} \langle f^*(t) f(t+\tau) \rangle\, e^{i\omega\tau}\, d\tau . \tag{3.12}$$

The second-order power spectrum and the intensity correlation function also form a Fourier transform pair,

$$S^{(2)}(\omega) = \int_{-\infty}^{\infty} G^{(2)}(\tau)\, e^{i\omega\tau}\, d\tau . \tag{3.13}$$

One therefore has

$$S^{(2)}(\omega) = \frac{I_{LO}}{c\varepsilon_0} [S_f(\omega - \omega_{AO}) + S_f(-\omega - \omega_{AO})] . \tag{3.14}$$

As was explained in section 2, for a given detection angle the spectrum $S_f(\omega)$

consists of one Rayleigh peak around $\omega = 0$, and two Brillouin peaks at $\omega = \pm\omega_c$, where ω_c is determined by the experimental geometry. So, if ω_{AO} is larger than ω_c, one has, for positive ω,

$$S^{(2)}(\omega) = \frac{I_{LO}}{c\varepsilon_0} S_f(\omega - \omega_{AO}) . \tag{3.15}$$

The second-order power spectrum of the detector signal is therefore equal to the power spectrum of the stochastic hydrodynamic fluctuations shifted by an amount ω_{AO}, independent of the phase fluctuations of the incident light.

In the present detection scheme, the signal $j_d(t)$ is sampled for a certain length of time and then a fast Fourier transform of $j_d(t)$ is performed. The resulting data points correspond to the magnitude of the Fourier transformed signal $j_d(t)$,

$$j_d(\omega) = \left| \int_{-\infty}^{\infty} j_d(t)\, e^{-i\omega t}\, dt \right| . \tag{3.16}$$

Since the signal $j_d(t)$ is a real quantity, one has

$$j_d^2(\omega) = \int_{-\infty}^{\infty} j_d(t')\, e^{-i\omega t'}\, dt' \int_{-\infty}^{\infty} j_d(t)\, e^{i\omega t}\, dt \propto \int_{-\infty}^{\infty} \langle j_d(t) j_d(t+\tau) \rangle\, e^{-i\omega t}\, dt . \tag{3.17}$$

Since the detector signal is proportional to the intensity, the correlation function appearing in expression (3.17) is proportional to the second-order correlation function (3.4). The squares of the computed data points therefore correspond precisely to the second-order spectrum of eq. (3.13), which in turn is equal to the (shifted) spectrum of the hydrodynamic fluctuations. This technique is simpler and more direct than the standard heterodyne techniques, where one either uses a spectrum analyser to measure the spectral density of the detector signal $j_d(\omega)$ or an autocorrelator to measure the signal autocorrelation function $\langle j_d(t) j_d(t+\tau) \rangle$.

4. Experimental setup and procedure

The liquid sample is contained in a carefully cleaned shallow glasss container of 0.1 m diameter, which is placed inside a sealed compartment, as shown in fig. 2. The outer compartment ($0.66 \times 0.25 \times 0.23\ m^3$) is made of black ano-

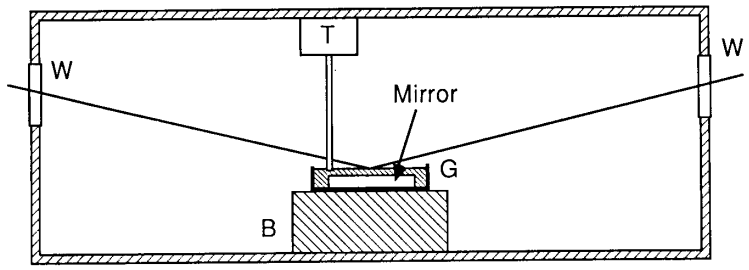

Fig. 2. Cell for observing the light scattering from liquid–vapor interfaces. The liquid sample is placed in a shallow glass dish (G) on an adjustable base (B). A high-quality mirror prevents the light beam that penetrates the liquid from scattering from the bottom of the glass dish into the direction of the detector. The thickness of the liquid layer on top of the mirror is about 0.5 mm. To align the detection a transducer (T) induces waves of a given frequency. The entire assembly is mounted in a vacuum tight chamber with windows (W) on each side.

dized aluminum and has two high quality windows on opposite sides. The composition and pressure of the gas within the enclosure can be controlled. The height of the interface can be adjusted with a micrometer. A 1–20 kHz transducer can excite surface waves of a given frequency for calibration purposes. Since long wavelength surface waves lower the resolution of the measurement, the measurements are usually carried out on thin samples of liquid (typically 0.5 mm). A high quality optical mirror covers the bottom surface of the container (see fig. 2), to reduce diffuse scattering of the light that penetrates the liquid.

To further prevent surface wave excitations by floor vibrations, the sample cell and the optical components are mounted on a vibration isolated platform. Vibration isolation is achieved in two ways. Vibrations above 100 Hz are damped by a rigid and massive (1000 kg) table supported by three air cylinders. A passive air servo systems keeps the the table top within 25 μm of the preset position. Further isolation is obtained by placing an actively stabilized platform (Newport electronic vibration isolation system) on top of the air-damped table. Stabilization is achieved with passive springs and an electromechanical servo system consisting of eight accelerometers and eight force transducers (one vertical and one horizontal in each of the four corners). The resulting stability is good enough to keep the specular beam from a liquid surface steady to within 60 μrad.

The optical arrangement is shown in fig. 3. A collimated 4 mW multimode He–Ne laser beam is split in two with a glass slide: 5% of the beam serves as a local oscillator, while the remainder illuminates the liquid surface inside the cell. Since background scattering greatly reduces the efficiency of a separate local oscillator beam, no optics are placed closer than 0.3 m from the liquid

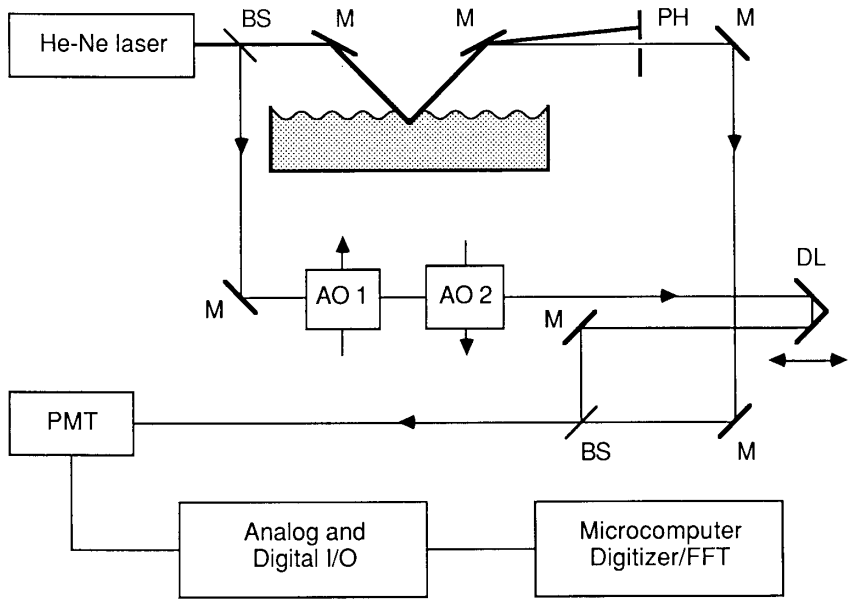

Fig. 3. Setup for measuring the light scattering from liquid–vapor interfaces. A multimode He–Ne laser beam is split in two: 95% of the beam scatters off the liquid–vapor interface, the remainder provides the local oscillator field. The local oscillator beam is frequency-shifted by two acousto-optic modulators (see text). After spatial filtering the scattered light and the local oscillator are combined again and the beats detected with a photomultiplier tube. The digitized signal is Fourier transformed on line by a microcomputer. The resulting datapoints correspond to the spectrum of the hydrodynamic fluctuations in the interface. M = mirror, BS = beam splitter, PH = pinhole, DL = delay line, AO = acousto-optic modulator.

surface and the external (instead of internal) surface reflection is used. The main beam strikes the surface under an incidence angle of about 80° with the vertical. The scattered light is picked up by a mirror. A set of 4 pinholes, aligned to make a small angle with the specular beam, further eliminates background scattering. The scattering angle, which determines the wavevector of the capillary waves observed, can be varied from 0–30 mrad. Residual table vibrations limit the accuracy of the scattering angle to about 60 μrad. The angle of view, determined by the opening of the pinholes, is about 0.1 mrad. The local oscillator and the scattering beam are recombined with a second glass slide and the combined beams are detected with a photomultiplier tube. Alignment is done by inducing a surface wave of a given frequency with a transducer and aligning the pinholes around the (visible) Bragg reflected beam.

To allow measurement of the spectrum at frequencies close to the frequency of the incident light, the frequency of the local oscillator is shifted by

acousto-optic modulation. Since the frequency shifts needed to allow separation of the up-shifted and down-shifted components of the light are much larger than the approximately 5 kHz shift desired, two 40 MHz acousto-optic crystals with a frequency difference of 4.9 kHz are used. The up-shifted component of the first crystal is used as input for the second one. The resulting frequency shift of the down-shifted component of the second crystal is then equal to the frequency difference between the drivers of the two acousto-optic crystals. The optical path length of the local oscillator beam can be adjusted with a small delay line to make it equal to the path length of the main beam. The coherence length of the laser light is about 0.2 m, corresponding to the 1 GHz laser bandwidth.

The photomultiplier signal is amplified and digitized at a 20 kHz rate by a GW Instruments MacAdios computer interface connected to an Apple Macintosh computer. The signal is sampled for about 200 ms, and the sampled waveform stored in the computer memory. Then a discrete fast Fourier transform is applied to the waveform. To improve the signal-to-noise ratio this procedure is repeated 50 times and the transform averaged. The spectral range of the measurements is limited to 10 kHz by the sampling rate of the digitizer.

5. Consistency checks

Spectral data are obtained in a variety of optical arrangements, shown in fig. 4, depending on the purpose of the measurement. Without local oscillator beam (fig. 4a) the light reaching the detector consists of surface Rayleigh and Brillouin light only, and the signal is small. The signal dramatically increases by mixing in some laser light at the detector, as is usually done in light-beating spectroscopy. This type of measurement, however, does not allow measurement of the spectrum near the laser frequency, i.e. at zero beat frequency. Moreover, the two Brillouin peaks fall on top of each other since both beat at ω_c. The experimental data reported here were obtained by frequency-shifting the local oscillator by an amount $\omega_{AO} > \omega_c$ (fig. 4b). The two Brillouin peaks then shift and separate, and the full Rayleigh–Brillouin triplet becomes visible (section 6).

In principle one also has contributions from light scattered by the apparatus and light scattered in the bulk liquid. Any such elastically scattered light reduces the efficiency of the shifted local oscillator. The contribution from instrumental scattering is minimized by extensive spatial filtering, and by making the bottom of the sample container highly reflective. Several checks are carried out to insure consistency of the measurements.

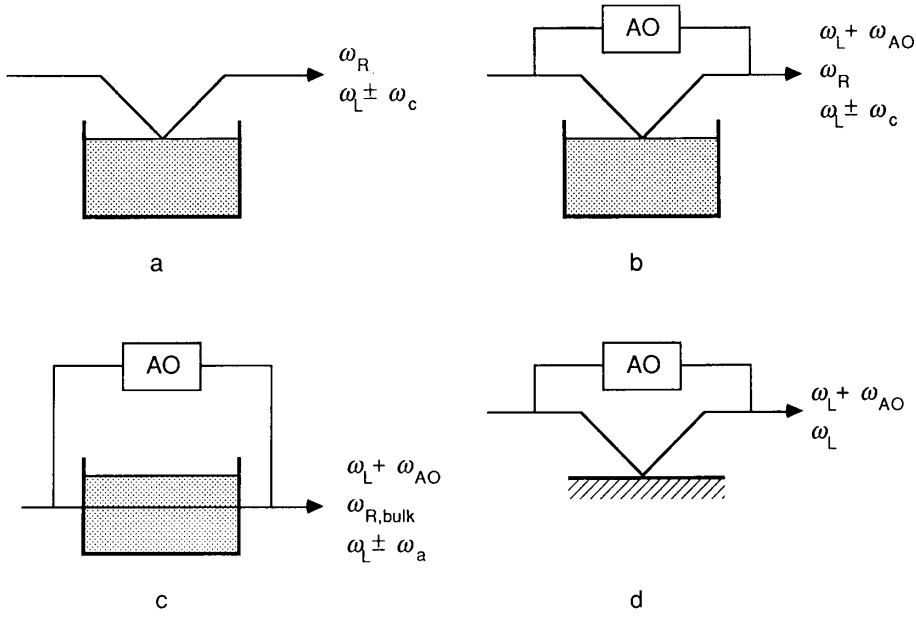

Fig. 4. Schematic diagram of the optical arrangements: (a) homodyne detection of surface scattering; heterodyne arrangement with shifted local oscillator for (b) surface and (c) bulk scattering; (d) arrangement for measuring instrumental contribution. AO = acousto-optic modulator, ω_L = incident laser light, $\omega_L \pm \omega_c$ = capillary wave scattering, $\omega_L \pm \omega_a$ = scattering from bulk acoustic waves.

a) *Bulk light scattering*. Fluctuations in the bulk liquid cause both Rayleigh scattering and Brillouin scattering from acoustic waves. Since a large portion of the incident beam penetrates the liquid, Rayleigh scattering from the bulk liquid will inevitably reach the detector. The detection angle for this scattering is roughly 90° (see Fig. 1). At this angle the bulk Rayleigh peak is about 10^3 times broader than the 10 kHz spectral range of the Fourier transform heterodyne detector and can therefore not be observed. Indeed, no scattered light from the bulk could be detected in the arrangement shown in fig. 4c at angles ranging from a few mrad to 90°.

b) *Instrumental light scattering*. The contribution of diffuse elastic scattering from the walls of the sample container and the optical components was examined by removing the liquid sample from the container. Without liquid the signal decreased by a factor 10^3 in intensity, and the spectrum showed only a very faint and narrow central peak.

c) *Alignment*. A further check was carried out by intentionally misaligning the

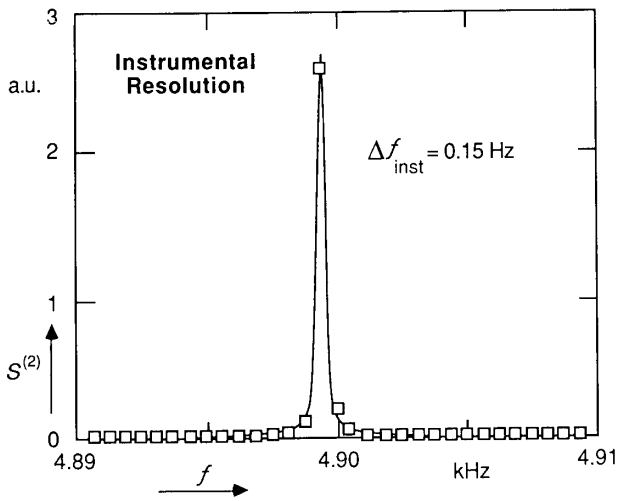

Fig. 5. Instrumental resolution of the Fourier transform heterodyne detection technique. This peak was obtained in the optical geometry shown in fig. 4d. The position of the peak is determined by the frequency shift of the local oscillator ω_{AO}. The half-width obtained from a Lorentzian fit to the data points is 150 mHz.

detection, with the detector viewing an area adjacent to the spot illuminated by the incident beam. No signal could be detected.

d) *Instrumental resolution*. By placing a mirror at the position of the liquid–vapor interface, and reducing the scattering angle α to zero, the instrumental resolution was measured (see fig. 4c). The reflected light beam was mixed with the shifted local oscillator and the resulting beat spectrum analyzed. The half-width of the instrumental line at ω_{AO} is roughly inversely proportional to the sampling time of the photomultiplier signal (i.e. the number of points sampled at a fixed sampling rate), up to a minimum of 0.15 Hz for a single 1.5 s sampling (see fig. 5). Increasing the sampling time beyond 1.5 s does not result in any further improvement in resolution. This limit is caused by frequency drifting of the acousto-optic driver, and by the spatial coherence quality of the laser beam.

6. Elastic and inelastic scattering from liquid–vapor interfaces

Measurements were carried out on water and ethanol at room temperature. Experimental results are shown in figs. 6–9. The first measurements were undertaken without frequency-shifting the local oscillator ($\omega_{AO} = 0$) in the

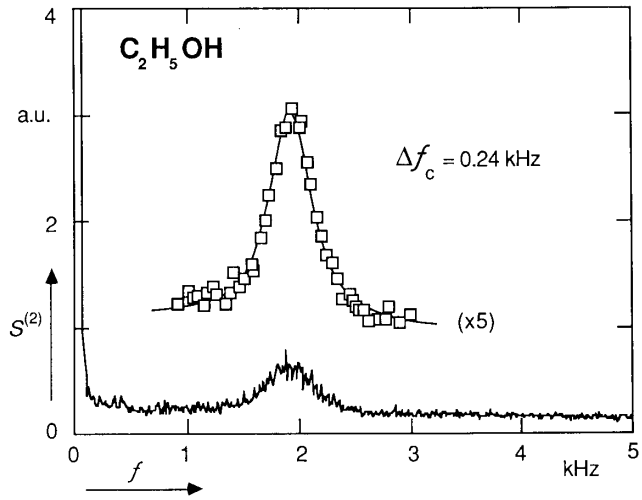

Fig. 6. Power spectrum of light scattered at an angle of 5 mrad from the liquid–vapor interface of ethanol at room temperature. The arrangement used is shown in fig. 4b with $\omega_{AO} = 0$. The points are experimental and the curve is a theoretical fit of a Lorentzian with a linear background. The half-width of the Lorentzian is 240 Hz.

arrangement shown in fig. 4b. The power spectrum of light scattered at an angle of 5 mrad from the liquid interface of ethanol is shown in fig. 6. When the local oscillator beam is blocked the signal becomes much weaker, but the spectrum of the "self-beating", or *homodyne*, signal from the main beam is identical to the one shown. The position of the peak is in good agreement with the published data for the surface tension and viscosity.

By frequency-shifting the local oscillator, the full Rayleigh–Brillouin triplet becomes visible (fig. 7). Note that this spectrum contains both a homodyne and a heterodyne component. The heterodyne component is centered around ω_{AO} at 4.9 kHz and consists of a central Rayleigh component and two Brillouin lines. The much weaker homodyne spectrum is centered around zero frequency; one can see the tail of the Rayleigh peak and a barely discernable Brillouin peak (see arrow). The apparent asymmetry in the height of the two Brillouin peaks is caused by a sloping background and by a nonlinearity of the digitizer. To prove that the Brillouin peaks are indeed of equal height, the sign of the frequency shift ω_{AO} was switched, so that the two Brillouin peaks exchange position. The resulting spectrum was identical to the one shown in fig. 7.

The two Brillouin peaks should correspond to two surface waves travelling in opposite direction: one along the direction of propagation of the light (+), and one in the opposite direction (−). The directional separation was confirmed as follows. First, the spectral purity of the local oscillator beam was checked: if

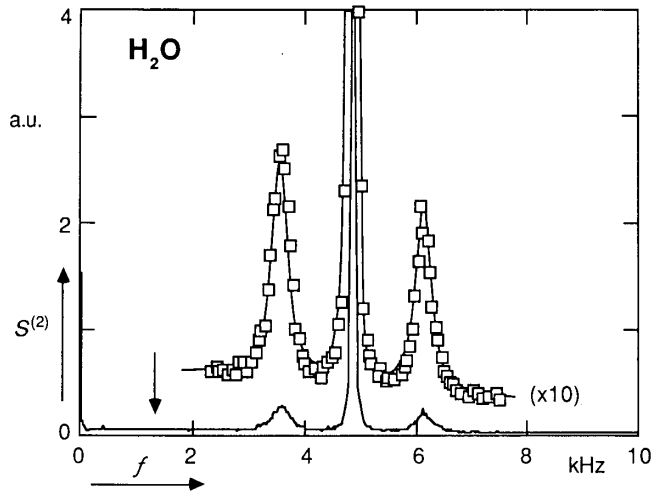

Fig. 7. Power spectrum of light scattered at an angle of 5 mrad from the liquid–vapor interface of water at room temperature with a sample thickness of about 0.5 mm. The arrangement used is shown in fig. 4b, with $\omega_{AO} = 4.9$ kHz. The full Rayleigh–Brillouin triplet is visible around ω_{AO}. The position of the homodyne Brillouin peak at 1.2 kHz is marked with an arrow. The curve through the data points is a best fit of three Lorentzians. The asymmetry in the height of the Brillouin peaks is caused by a nonlinearity in the digitizer.

some down-shifted light at $\omega_L - \omega_{AO}$ reaches the detector in addition to the up-shifted light at $\omega_L + \omega_{AO}$, only partial separation results. Therefore, before every experiment the homodyne spectrum of the local oscillator beam was measured, and verified to have no spectral lines. As a further check the experiments were carried out on induced (unidirectional) surface waves. The direction of the induced wave can be inverted by changing the position of the transducer (see fig. 2). The result is shown in figs. 8a and 8b. In fig. 8a an induced wave of frequency $\omega_{ind} = 1$ kHz is co-propagating with the laser light. The heterodyne spectrum contains now only two peaks: one Rayleigh peak at $\omega_{AO} = 4.9$ kHz and one single Brillouin peak at $\omega_{AO} - \omega_{ind}$. Notice also the strong homodyne peak at ω_{ind}. When the direction of the induced wave is reversed the other Brillouin peak appears, see fig. 8b. The graphs clearly show that the present technique entirely separates counter-propagating capillary waves. Without a shifted local oscillator the spectra remain identical (see homodyne part).

The width of the spectral lines in figs. 6 and 7 is determined by the spectral and angular resolution, Doppler broadening, and finally the natural linewidth. Different mechanisms are responsible for the observed widths of the Rayleigh and Brillouin peaks.

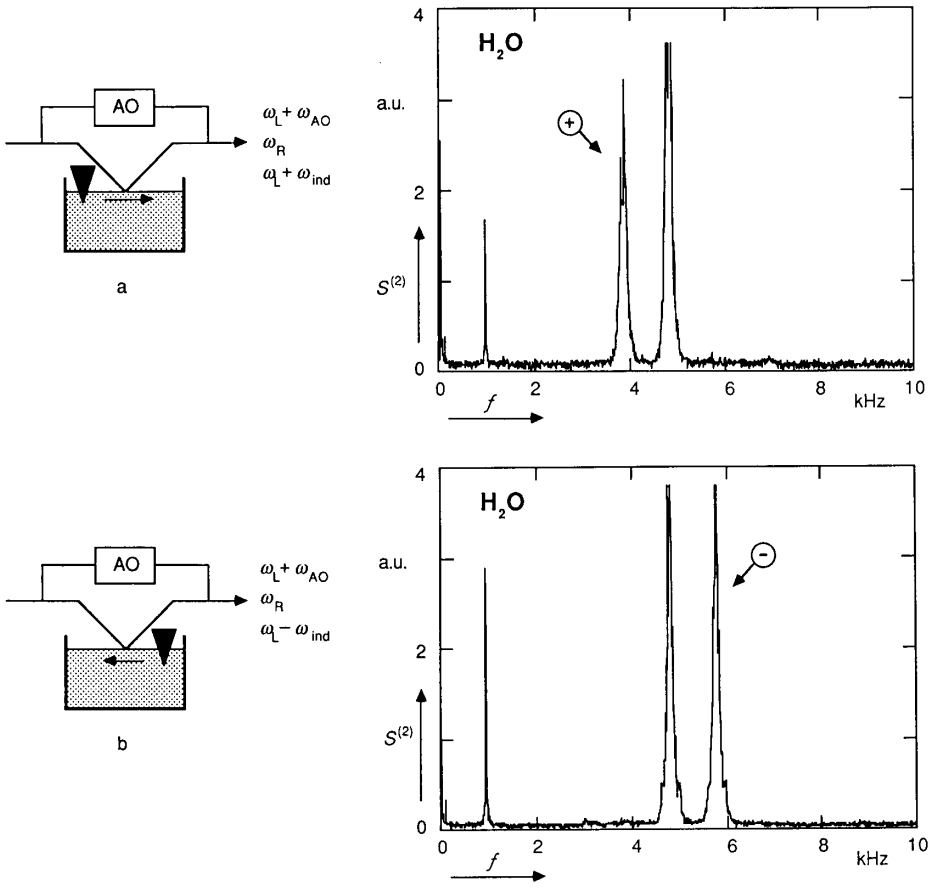

Fig. 8. Check of the directional separation. A co-propagating (a) or counter-propagating (b) unidirectional wave of frequency $\omega_{ind} = 1$ kHz is induced on the liquid surface by a transducer (black triangle) as shown in the diagrams on the left. In both cases the heterodyne spectrum shows only one Brillouin peak. Notice that the *homodyne* peak, which corresponds to a beating of ω_R with $\omega_{AO} \pm \omega_{ind}$, does not change.

Spectral resolution. The spectral resolution was discussed in section 5. For a single sampling the resolution is better than 0.2 Hz. For multiple samplings some degradation in resolution was observed owing to small drifts in the acousto-optic driver. Under all circumstances the spectral resolution was better than 5 Hz.

Angular resolution. The angular resolution of the scattering angle α (fig. 1) is limited by table vibrations, by the opening of the pinholes, and by the divergence of the laser beam. This will lead to a spread in wavevector for the

observed surface vibrations. With the active stabilization the angular variations because of table vibrations are negligible. The pinholes limit the angular resolution to about 0.1 mrad, while the divergence of the laser beam is about 0.5 mrad. For small scattering angles of a few mrad the combined effect can result in a 10% spread in wavevector.

Doppler broadening. Long-wavelength surface waves produced by residual table vibrations cause the interface to move up and down, which in turn results in a Doppler-broadening of the signals. This broadening was measured directly by reducing the scattering angle α to zero and observing the spectrum of the reflected light. For liquid samples 15 mm deep a Doppler broadening of about 50 Hz was observed, see fig. 9. By reducing the thickness of the liquid samples the long-wavelength gravity waves can be suppressed. Indeed, by reducing the sample thickness to 0.5 mm the Doppler broadening disappears.

Natural line width. The natural line width of the spectral lines is determined by the damping term in the dispersion relation. For the Brillouin peaks the width can be obtained from eq. (2.3). Although very few accurate experimental data

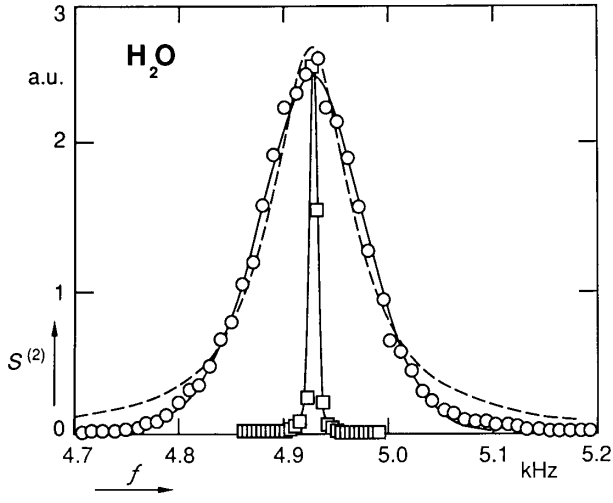

Fig. 9. Central Rayleigh peak of the spectrum of light scattered at an angle of 5 mrad from the liquid–vapor interface of water at room temperature. The squares correspond to the central line shown in fig. 7. The solid curve through these points is a least square fitted Lorentzian of half-width 5 Hz. In a sample of 15 mm thickness (circles) the line broadens due to motion of the interface. Lorentzian (dashed) and Gaussian (solid) curve fittings are shown. The half-width of the Gaussian curve is 50 Hz.

for the width of the Brillouin peaks are available, recent experiments have extensively measured the line width for capillary waves on ethanol, and verified the correctness of the theoretical predictions[29,30]). If the central Rayleigh peak in the spectrum in fig. 6 is a result of light scattering from the nonpropagating modes discussed in section 2, then the width of the peak should be determined by eq. (2.2). No data are available for the coefficient of sliding friction β appearing in that expression.

In the experiments reported here the scattering angle α is much smaller than in previous experiments, and the frequency of the observed capillary waves much lower. For a capillary wave with $\omega_c = 1$ kHz, the expected linewidths are 114 and 38 Hz for ethanol and water, respectively. The angular resolution of the present apparatus, however, causes a considerable spread in the frequency of the observed capillary waves. We must therefore conclude that the observed widths of the (low frequency) thermally excited capillary wave peaks are determined by instrumental broadening. For higher frequency ($\omega_c > 10$ kHz) capillary waves this complication does not arise, since the lines are much broader, and, at the same time, the relative spread in wavevector much smaller because of the larger scattering angle α. To observe capillary waves at higher frequencies, while still maintaining the condition $\omega_{AO} > \omega_c$ (see eq. 3.15), one needs a sampling rate higher than the current one. We plan to implement this in our apparatus in the near future.

The Rayleigh line is about forty times narrower than the Brillouin lines. The presence of this line was checked for scattering angles ranging from close to 0 mrad to 30 mrad. The consistency tests described in section 5 prove that the scattered light corresponding to this peak cannot be caused by scattering from the bulk liquid or vapor phases, or by instrumental scattering. Moreover, the width of this line depends on the motion of the surface: for a thin layer of about 0.5 mm the line is narrow and nearly Lorentzian. For a thicker layer it broadens and becomes Gaussian because of Doppler broadening (see fig. 9). One must therefore conclude that the origin of this scattering lies in the liquid–vapor interface. Although we cannot completely rule out the presence of impurities *at the interface*, we believe that if impurities were responsible for this scattering the measurements would not reproduce from one sample to another, and from one sample container to another. If one uses an upper limit of 10 Hz for the natural line width of the central line, one finds an upper limit of 0.04 kg s^{-1} m^{-2} for β using eq. (2.2). A rough estimate of β from $\beta \approx \eta^i / d^i$, with $d^i \approx 1$ nm the interface thickness, however, yields a value which is four orders of magnitude larger, even when taking $\eta^i \approx \eta^v$. We therefore conclude that the observed mode cannot be the one considered in the analysis in ref. 6, and can only be accounted for by a much slower mechanism.

7. Concluding remarks

This paper presents the first of a still incomplete series of experiments on light scattering from liquid–vapor interfaces. The measurements, for the first time, resolve the full Rayleigh–Brillouin triplet. Many improvements are being made to the present apparatus. In addition to a systematic investigation of liquid–vapor interface spectra using the above technique, experiments to measure the predicted asymmetry in the Brillouin spectrum are in progress. Because of the directional separation Fourier transform heterodyne spectroscopy is particularly well suited to study nonequilibrium effects. We also plan to study liquid–liquid interfaces and the effect of surfactants on liquid–vapor interfaces.

Acknowledgments

This work was in part supported by a grant from the Division of Applied Sciences at Harvard University and by the Newport Corporation. The experiments resulted from discussions with professors R. Desai and I. Oppenheim. We are indebted to Ka Yee Lee for her valuable help with the experiments. We are also pleased to acknowledge useful discussions with professors D. Bedeaux, B.I. Halperin, P. Mazur and Dr. W. van Saarloos.

References

1) J.D. van der Waals, Z. Phys. Chem. **13** (1894) 657.
2) L.D. Landau and E.M. Lifshitz, Fluid Mechanics (Pergamon, New York, 1959).
3) V.G. Levich, Physicochemical Hydrodynamics (Prentice-Hall, New Jersey, 1962).
4) R. Loudon, in: Surface Excitations, V.M. Agranovich and R. Loudon, ed. (Elsevier, Amsterdam, 1984), p. 589.
5) D. Bedeaux, A.M. Albano and P. Mazur, Physica **82A** (1976) 438.
6) D. Bedeaux and I. Oppenheim, Physica **90A** (1978) 39.
7) D. Ronis and I. Oppenheim, Physica **117A** (1983) 317.
8) See, for instance, the review articles in Physics Today **37** (1984).
9) S.R. de Groot and P. Mazur, Nonequilibrium Thermodynamics (Dover, New York, 1984).
10) D. Ronis, I. Procaccia and I. Oppenheim, Phys. Rev. A **19** (1979) 1324.
11) G. van der Zwan, D. Bedeaux and P. Mazur, Physica **107A** (1981) 491.
12) T.R. Kirkpatrick, E.D.G. Cohen and J.R. Dorman, Phys. Rev. A **26** (1982) 950, 972, 995.
13) D. Beysens, Y. Garrabos and G. Zalczer, Phys. Rev. Lett. **45** (1980) 403.
14) H. Kiefte, M.J. Clouter and R. Penny, Phys. Rev. B **30** (1984) 4017.
15) M. Grant and R. Desai, Phys. Rev. A **27** (1983) 2577.
16) R. Desai and M. Grant, in: Fluid Interfacial Phenomena, C.A. Croxton, ed. (Wiley, New York, 1986), p. 135.

17) H.Z. Cummins and H.L. Swinney, Progress in Optics, vol. 8 (North-Holland, Amsterdam, 1970), chap. 2.
18) R.H. Katyl and U. Ingard, Phys. Rev. Lett. **20** (1968) 248.
19) M.A. Bouchiat, J. Meunier and J. Brossel, C.R. Acad. Sc. Paris **266B** (1968) 255.
20) M.A. Bouchiat and J. Meunier, C.R. Acad. Sc. Paris **266B** (1968) 301.
21) M.A. Bouchiat and J. Meunier, J. Physique **33** (1972) C1-141.
22) E.S. Wu and W.W. Webb, J. Physique **33** (1972) C1-149.
23) E.S. Wu and W.W. Webb, Phys. Rev. A **8** (1973) 2077.
24) H.Z. Cummins, N. Knable and Y. Yeh, Phys. Rev. Lett. **12** (1964) 150.
25) N.A. Clark, J.H. Lunacek, and G.B. Benedek, Am. J. Phys. **38** (1970) 575.
26) See, for instance, I.L. Fabelinskii, Molecular Scattering of Light (Plenum, New York, 1968).
27) J. Vlieger and D. Bedeaux, Physica **82A** (1976) 221.
28) J.C. Brown, Am. J. Phys. **51** (1983) 1008.
29) L.B. Shih, Rev. Sci. Instrum. **55** (1984) 716.
30) J.A. Mann and R.V. Edwards, Rev. Sci. Instrum. **55** (1984) 727.